

Supporting information

Modulation of Intermolecular Interaction in Hole Transporting Materials for Improvement of Perovskite Solar Cell Efficiency: A Strategy of Trifluoromethoxy Isomerization

Jiayi Qi,^a Ruiqin Wang,^a Xin Chen,^a Fei Wu,^{b,*} Wei Shen,^a Ming Li,^a Rongxing He,^{a,*} and Xiaorui Liu^{a,*}

^a Chongqing Key Laboratory of Soft-Matter Material Chemistry and Function Manufacturing, School of Chemistry and Chemical Engineering, Southwest University, Chongqing 400715, P.R. China

^b Chongqing Key Laboratory for Advanced Materials and Technologies of Clean Energy, School of Materials and Energy, Southwest University, Chongqing 400715, P. R. China

* Corresponding authors and E-mail: feiwu610@swu.edu.cn (F. Wu); herx@swu.edu.cn (R. He); liuxiaorui@swu.edu.cn (X. Liu)

1. Experimental Section

1.1 Computational Details

The ground-state geometry for investigated molecules JY4-JY6 were optimized using the B3P86/6-311G(d, p) functional and basis set.^{1,2} The energies of all obtained geometries are ensured to be the lowest because the optimized structures do not exhibit imaginary frequency. On basis of the B3P86/6-311G(d, p) levels, the values of HOMO and LUMO energy levels for JY4-JY6 were calculated.

Moreover, energy calculations, including electron affinities, adiabatic ionization potential of the investigated HTMs were performed using the B3P86/6-311G(d, p) method and basis set. On basis of the ground-state geometry, the optical properties of JY4-JY6 were calculated by TD-PBE0/6-31G(d) functional and basis set in dichloromethane solution with a polarizable continuum model (PCM). The reorganization energy of an organic molecule consists of inner recombination energy and outer recombination energy. The inner recombination energy is defined as the deformation in the nuclear coordinates from initial to final coordinates. For most organic molecules, outer recombination energy is small and often neglected. Therefore, inner recombination energy for hole was calculated in this work. The parameter of λ_h was obtained from the adiabatic potential energy surfaces method with the level of B3P86/6-311G(d, p). The DFT and TD-DFT calculations were carried out by the Gaussian 09 program.³

Molecular dynamics (MD) simulation was performed using the Gromacs program.⁴ Simulations were carried out under NPT system conditions of 298.15 K, time step of 1 fs, Berendsen pressure coupling (reference pressure 1 Bar, pressure control time constant 1 ps, compression ratio $4.5 \times 10^5 \text{ bar}^{-1}$) and velocity scale temperature coupling (time-temperature control constant 0.2 ps). The Particle Mesh Ewald (PME) method was used to calculate the electrostatic interaction, considering the remote correction of the van der Waals interaction, and the cutoff value was set to 1.0 nm. In the whole simulation process, GAFF force field was used, and RESP charge was obtained through DFT optimization of HTMs,^{5,6} DFT optimization under B3P86/6-311G(d,p) was carried out using Gaussian09 program, and simulation results were visualized using VMD program. The simulation process is assisted by the Multiwfn program.^{7,8}

The core of Marcus charge transfer theory is the Marcus equation.⁹ In the context of perovskite solar cells, the hole transport layer primarily facilitates hole transport. Therefore, the Marcus theory is used to describe the transport behavior of holes or electrons, and their charge transfer rate (k) can be expressed as:

$$k = \frac{4\pi^2}{h} V^2 \frac{1}{\sqrt{4\pi\lambda k_B T}} \exp\left[-\frac{\lambda}{4k_B T}\right] \quad \text{S-1}$$

Where h represents the Planck constant, k_B denotes the Boltzmann constant, T signifies the temperature (measured in Kelvin), and λ represents the hole recombination energy calculated from the absolute potential energy surface:¹⁰

$$\lambda = (E_0^* - E_0) + (E_+^* - E_+) \quad \text{S-2}$$

Here, E_+^* and E_0^* respectively denote the total energy of the charge state on the optimal neutral structure and the optimal charge state structure, each having neutral and cationic matter geometries. E^+ and E^0 represent the total energy of the optimal molecular configuration for the neutral state and the charge state, respectively. V signifies the intermolecular electron coupling between two adjacent molecules in the structure, as indicated by the following formula:¹¹

$$V = \frac{J_{RP} - S_{RP}(H_{RR} + H_{PP})/2}{1 - S_{RP}^2} \quad \text{S-3}$$

Here, H_{RR} and H_{PP} are lattice energies, S_{RP} is the overlap integral, and J_{RP} represents the transfer integral of dimers in non-adiabatic states.

The hole mobility of the hole transport materials is calculated using the Einstein relation as follows:¹²

$$\mu = \frac{1}{2nk_B T} \sum_i e r_i^2 k_i P_i \quad \text{S-4}$$

Here, n represents the spatial dimension. In this context, we are considering the selection of hole transport pathways in three-dimensional space. i denotes a specific transport pathway, r_i represents the center-of-mass distance between hole transport dimers, k_i denotes the hole transition rate. P_i is defined as the relative transition probability for the hole to transition to pathway i and can be determined using the following equation:

$$P_i = \frac{k_i}{\sum_i k_i} \quad \text{S-5}$$

The electronic coupling could be simulated from the PW91/TZP levels in ADF program.^{13,14}

The distribution and arrangement of HTMs on perovskite surface were observed by MD simulation. We used the (0 0 1) plane as the model for the perovskite surface, constructing a $7 \times 7 \times 3$ perovskite cell with a 95 Å vacuum region surrounding the external PbI_2 layer. The dimensions of the surface model box were $44.5 \times 44.5 \times 95.0$ Å. At 0 ns, the HTMs were randomly distributed across the perovskite surface structure. During the simulation, the HTMs spontaneously adsorbed onto the perovskite surface, with each cell containing 24 HTM molecules. The simulations were conducted under NVT ensemble conditions, including temperature of 300 K, time step of 1 fs, and time-temperature control constant of 0.2 ps. The Particle Mesh Ewald (PME) method was utilized for calculating electrostatic interactions, accounting for van der Waals long-range corrections with a cutoff value set at 1.2 nm. To mimic real device fabrication conditions, an annealing process was implemented, starting from an initial system temperature of 0 K, ramping up to 400 K within 100 ps, maintaining 400 K for 500 ps, and finally cooling down to 300 K within 100 ps until the end of the simulation.

The systems of perovskite/HTMs (JY4-JY6) interfaces were optimized employing the generalized gradient approximation (GGA) with Perdew-Burke-Ernzerhof (PBE) exchange-correlation functional in Vienna ab initio simulation program (VASP).¹⁵⁻¹⁸ It's reported that the

calculations have determined that the FAPbI_3 (0 0 1) plane is the most stable plane. During the simulation of HTM deposition, we selected the molecule closest to the perovskite surface for studying its adsorption state. In the calculation process, to mitigate the increase in time cost, we excluded the lower two layers of perovskite. The electronic wave functions were expanded by plane waves up to a kinetic energy cutoff of 400 eV. For k-point sampling, a $1 \times 1 \times 1$ Monkhorst-Pack grid was applied in the irreducible Brillouin zone. A 35 Å vacuum area was embedded into the outer PbI_2 surfaces to avoid unwanted interactions. The convergence threshold for self-consistent iteration was set at 1.0×10^{-4} eV/atom, and the atomic positions were fully relaxed until the maximal force on each atom was less than 0.05 eV/Å. The adhesive energy (E_{ads}) was calculated using the following equation: $E_{\text{ads}} = E_{\text{PVK/HTM}} - E_{\text{PVK}} - E_{\text{HTM}}$. Non-self-consistent calculations were then performed and the charge density file was processed into a charge difference density (CDD) map.

1.2 Device Fabrication

To measure the photovoltaic performance of PSCs, a structure of $\text{FTO/TiO}_2/\text{Cs}_{0.05}\text{FA}_{0.85}\text{MA}_{0.10}\text{Pb}(\text{I}_{0.88}\text{Br}_{0.04}\text{Cl}_{0.08})_3/\text{HTMs/Ag}$ were fabricated. The patterned FTO glass (7Ω per square) were cleaned sequentially washed with detergent, deionized water, acetone, isopropanol in an ultrasonic bath and then dried by flowing air. The compact layer of TiO_2 was prepared by spray pyrolysis of solution (2 M acetylacetone and 0.2 M titanium isopropoxide in isopropanol) on the cleaned FTO substrate at 450 °C for 30 min. Then the FTO substrates were transferred into N_2 glovebox. A mixture of 1.63 M PbI_2 , 1.32 M FAI , 0.31 M MACl , 0.16 M MABr , 0.08 M CsI were dissolved in mixed solution (1 mL) of DMF and DMSO (V:V = 4:1). The mixed perovskite precursor is stirred for 12 h in N_2 glovebox. The perovskite film was deposited by a consecutive two-step spin-coating process at 2000 rpm for 10 s and then at a speed of 6000 rpm for 30 s on the surface of TiO_2 layer. At the time of 15 s prior to the program end, 200 μL of chlorobenzene was dripped on the spinning substrate, and then the film was annealed at 120 °C for 20 min. The film thicknesses of hole transport material for JY4-JY6 in PSC devices were roughly optimized on basis of various concentrations (40, 50 and 60 mg/mL, respectively). For the JY4 in the concentrations 40, 50 and 60 mg/mL, the PCEs of PSC devices are 17.42% (V_{OC} : 1.004 V, J_{SC} : 24.29 mA/cm^2 , and FF : 71.43%), 18.84% (V_{OC} : 1.034 V, J_{SC} : 24.08 mA/cm^2 , and FF : 75.64%), and 18.24% (V_{OC} : 1.022 V, J_{SC} : 24.04 mA/cm^2 , and FF : 74.24%), respectively. For the JY5 in the concentrations 40, 50 and 60 mg/mL, the PCEs of PSC devices are 19.33% (V_{OC} : 1.075 V, J_{SC} : 24.29 mA/cm^2 , and FF : 74.12%), 20.94% (V_{OC} : 1.077 V, J_{SC} : 24.15 mA/cm^2 , and FF : 80.51%), and 20.32% (V_{OC} : 1.079V, J_{SC} : 24.18 mA/cm^2 , and FF : 77.88%), respectively. For the JY6 in the concentrations 40, 50 and 60 mg/mL, the PCEs of PSC devices are 20.37% (V_{OC} : 1.072 V, J_{SC} : 24.40 mA/cm^2 , and FF : 77.88%), 22.06% (V_{OC} : 1.100 V, J_{SC} : 24.46 mA/cm^2 , and FF : 81.99%), and 21.28% (V_{OC} : 1.120 V, J_{SC} : 24.07 mA/cm^2 , and FF : 78.94%), respectively. The hole transport material solution was prepared by dissolving 50 mg of HTMs (JY4, JY5, JY6) in 1mL of CB, with the additives of 29.9 μL t-BP, 18.2 μL Li-TFSI. The HTMs solution was spin-coated on the perovskite film at 4000 rpm for 30 s. Finally, 100 nm thick Ag film was thermally evaporated on

the HTL in vacuum environment ($<10^{-5}$ Pa) to accomplish the whole fabrication of device. The active area of our device is 0.06 cm^2 .

1.3 The space-charge-limited current (SCLC) hole mobility measurements.

Hole-only devices are fabricated with the structure ITO/PEDOT:PSS/HTM/Ag. The dark J - V characteristics of hole-only devices were measured under N_2 atmosphere inside a glove box. PEDOT:PSS was deposited on the ITO substrate at 5000 rpm for 30 s, followed by annealing at 120°C for 30 min. The conditions of spin coating for HTMs are in consistent with the device fabrication. Mobility is extracted by fitting the current density-voltage curves using space charge limited current (SCLC) on basis of the following equation $J = 9\varepsilon_\theta\varepsilon_\gamma\mu_h V^2/8L^3$, where J is the current density, L is the film thickness, μ_h is the hole mobility, ε_γ is the relative dielectric constant of the transport medium ($\varepsilon_\gamma = 3$ for organic materials), ε_θ is the permittivity of free space ($8.85 \times 10^{-12} \text{ F m}^{-1}$), V is the internal voltage of the device.

1.4 Measurements

The ^1H nuclear magnetic resonance (^1H NMR) spectra were obtained from a BRUKER AVANCE NEO 400 MHz NMR Instrument (in DMSO-d_6 , 99.8%, Beijing Hwrkchemical Co., Ltd.). The ^{13}C nuclear magnetic resonance (^{13}C NMR) spectra were obtained from a BRUKER AVANCE NEO 151 MHz NMR Instrument (in CDCl_3 , 99.8%, Shanghai Meryer Technologies Co., Ltd.). Mass spectra were collected on a Bruker impact II high-resolution mass spectrometer. UV-vis absorption spectra were measured on a Shimadzu UV-2450 absorption spectrophotometer. Absorption spectra in solution were recorded in dichloromethane solution with a HTM concentration of 10^{-5} . Cyclic voltammetry studies were conducted using a CHI660E system in a typical three-electrode cell with a glass carbon working electrode, a platinum wire counter electrode, and a silver/silver chloride (Ag/AgCl) reference electrode. All electrochemical experiments were carried out under a nitrogen atmosphere at room temperature in an electrolyte solution of 0.1 M tetrabutylammonium hexa-fluorophosphate (Bu_4NPF_6) in dichloromethane at a sweeping rate of 50 mV s^{-1} . The potential of Ag/AgCl reference electrode was internally calibrated by using the ferrocene/ferrocenium redox couple (Fc/Fc^+). According to the onset oxidation potential of the CV measurements, the highest occupied molecular orbital (HOMO) was estimated based on the vacuum energy level of ferrocene (5.1 eV): $\text{HOMO} = -(\text{E}_{\text{onset}} - \text{E}_{\text{Fc}/\text{Fc}^+}) - 5.1 \text{ eV}$. The valence band (VB) energy levels and band gap (E_g) of the perovskite were determined using ultraviolet photoelectron spectroscopy (UPS) and ultraviolet-visible-near-infrared spectrophotometry (UV-Vis-NIR). UPS data for perovskite and JY4-JY6 film were obtained using the ThermoFisher ESCALAB 250Xi, and UV-Vis-NIR spectroscopy data were obtained using the Cary 5000 instrument. The current-voltage (J - V) curves were measured under 100 mW cm^{-2} (AM 1.5 G) simulated sunlight using Keithley 2400 in conjunction with a Newport solar simulator (94043A). Film thickness of hole transport layer and perovskite layer were measured by Surfcoorder ET200A, Kosaka Laboratory Ltd. Using atomic force microscopy (AFM) to characterize the morphology, the model is CSPM5500A. Steady-state PL spectra were recorded on Fluorolog®-3 fluorescence spectrometer (Horiba). Time-resolved PL

decay curves were measured by a single photon counting spectrometer from Horiba Instruments (Fluorolog®-3) with a Picosecond Pulsed UV-LASTER (LASTER375) as the excitation source. The cross-sectional of the device was characterized using Japan Hitachi SU-4800 field-emission scanning electron microscope (FE-SEM). Grazing incident wide-angle X-ray scattering (GIWAXS) test uses the Eiger2R 1M detector.

1.5 Synthetic route

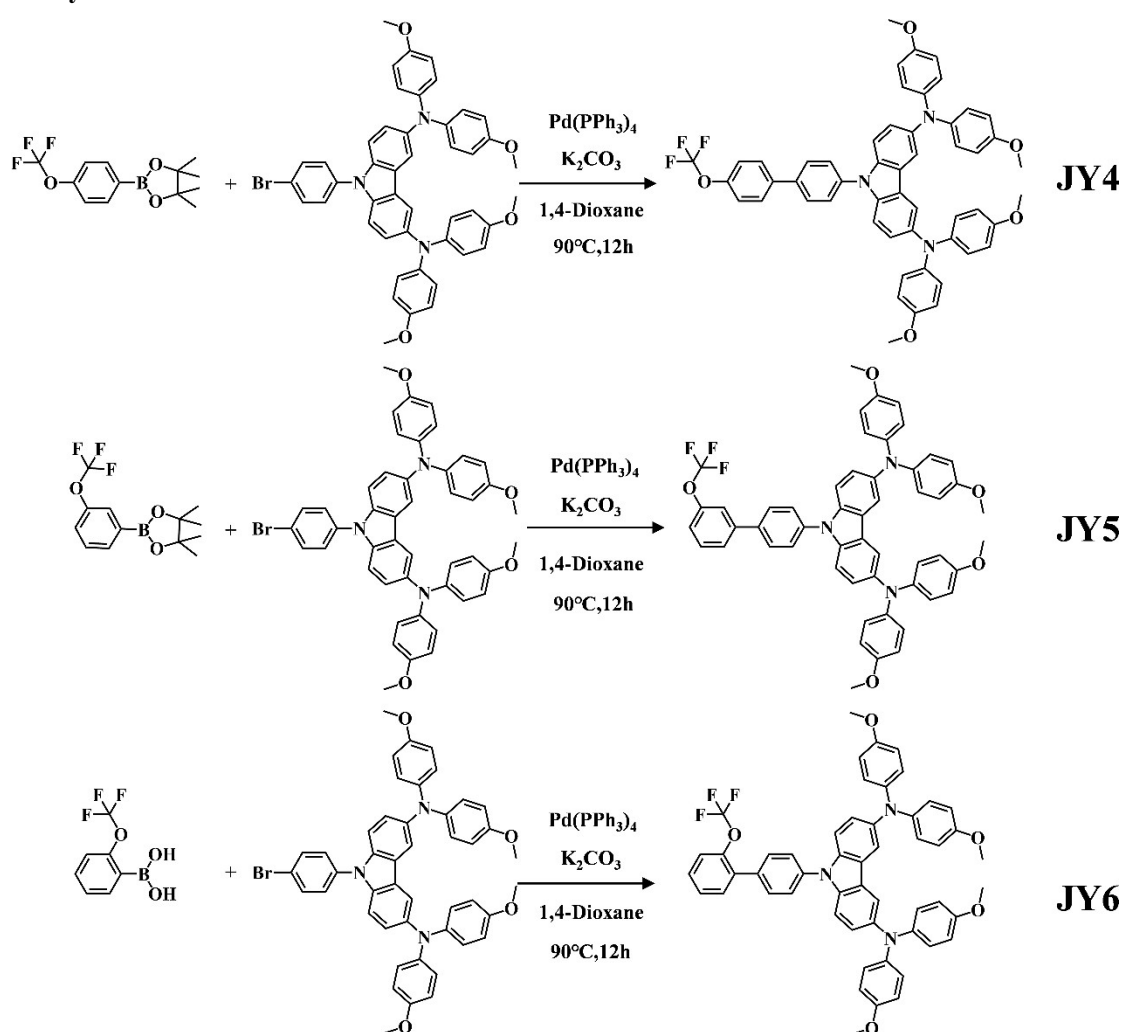


Figure. S1 Synthesis route of HTMs.

1.6 Synthesis of HTMs

The synthesis route of JY4-JY6 is shown in Figure. S1. JY4-JY6 were synthesized by Suzuki-Miyaura coupling reaction.

N^3,N^3,N^6,N^6 -tetrakis(4-methoxyphenyl)-9-(4'-(trifluoromethoxy)-[1,1'-biphenyl]-4-yl)-9H-carbazole-3,6-diamine (JY4): The 4,4,5,5-tetramethyl-2-(4-(trifluoromethoxy)phenyl)-1,3,2-dioxaborolane (93.68 mg, 0.32 mmol) and 9-(4-bromophenyl)- N^3,N^3,N^6,N^6 -tetrakis(4-methoxyphenyl)-9H-carbazole-3,6-diamine (209.3 mg, 0.27 mmol) were accurately weighed and putted into a round-bottomed flask (250 mL). The connected instrument was replaced by vacuum extraction for three times to fill the device with argon gas. Under argon atmosphere, the catalyst

Pd(PPh₃)₄ (0.027 mmol, 31.2 mg) was transferred to the flask. Pre-deoxygenated 1,4-dioxane (15 mL) solution and K₂CO₃ (2 M 1.5mL) solution were injected into the flask. The reaction was reflux at 90 °C for 12 h. After monitoring the reaction, the system was cooled to room temperature, extracted with dichloromethane (DCM), and dried with anhydrous Na₂SO₄ for 3 h. After vacuum extraction and filtration, the most of the solvent was removed using a rotary evaporator. Finally, the crude product was purified by column chromatography on silica gel (eluent: EA:PE = 1:5) to obtain white solid powder (185.7 mg, yield: 74.28%). ¹H NMR (600 MHz, DMSO) δ 7.97, 7.95, 7.92, 7.91, 7.74, 7.72, 7.52, 7.50, 7.49, 7.37, 7.36, 7.16, 7.15, 7.10, 7.09, 6.89, 6.88, 6.83, 6.82, 3.70, 3.33. ¹³C NMR (151 MHz, DMSO) δ 154.81, 148.53, 142.39, 141.88, 139.03, 138.05, 137.46, 137.17, 129.16, 128.94, 127.46, 124.95, 124.45, 124.00, 122.94, 122.01, 116.95, 116.68, 115.16, 111.26, 55.64.

***N*³,*N*³,*N*⁶,*N*⁶-tetrakis(4-methoxyphenyl)-9-(3'-(trifluoromethoxy)-[1,1'-biphenyl]-4-yl)-9*H*-carbazole-3,6-diamine (JY5):** The 4,4,5,5-tetramethyl-2-(3-(trifluoromethoxy)phenyl)-1,3,2-dioxaborolane (145.6 mg, 0.50 mmol) and 9-(4-bromophenyl)-*N*³,*N*³,*N*⁶,*N*⁶-tetrakis(4-methoxyphenyl)-9*H*-carbazole-3,6-diamine (271.3 mg, 0.35 mmol) were accurately weighed and putted into a round-bottomed flask (250 mL). The connected instrument was replaced by vacuum extraction for three times to fill the device with argon gas. Under argon atmosphere, the catalyst Pd(PPh₃)₄ (0.035 mmol, 40.5 mg) was transferred to the flask. Pre-deoxygenated 1,4-dioxane (15 mL) solution and K₂CO₃ (2 M 2.0 mL) solution were injected into the flask. The reaction was reflux at 90 °C for 12 h. After monitoring the reaction, the system was cooled to room temperature, extracted with dichloromethane (DCM), and dried with anhydrous Na₂SO₄ for 3 h. After vacuum extraction and filtration, the most of the solvent was removed using a rotary evaporator. Finally, the crude product was purified by column chromatography on silica gel (eluent: EA:PE = 1:5) to obtain white solid powder (250.7 mg, yield: 83.55%). ¹H NMR (600 MHz, DMSO) δ 8.00, 7.99, 7.85, 7.84, 7.77, 7.73, 7.72, 7.67, 7.66, 7.64, 7.43, 7.41, 7.37, 7.36, 7.10, 7.09, 6.89, 6.88, 6.87, 6.83, 6.82, 3.69, 3.32, 2.50. ¹³C NMR (151 MHz, DMSO) δ 154.83, 149.55, 142.39, 142.07, 141.91, 137.71, 137.44, 131.53, 129.06, 127.50, 126.37, 124.97, 124.46, 124.03, 119.81, 116.97, 115.18, 111.28, 55.65, 55.63.

***N*³,*N*³,*N*⁶,*N*⁶-tetrakis(4-methoxyphenyl)-9-(2'-(trifluoromethoxy)-[1,1'-biphenyl]-4-yl)-9*H*-carbazole-3,6-diamine (JY6) :** The (2-(trifluoromethoxy)phenyl)boronic acid (108.2 mg, 0.53 mmol) and 9-(4-bromophenyl)-*N*³,*N*³,*N*⁶,*N*⁶-tetrakis(4-methoxyphenyl)-9*H*-carbazole-3,6-diamine (271.3 mg, 0.35 mmol) were accurately weighed and putted into a round-bottomed flask (250 mL). The connected instrument was replaced by vacuum extraction for three times to fill the device with argon gas. Under argon atmosphere, the catalyst Pd(PPh₃)₄ (0.035 mmol, 40.44 mg) was transferred to the flask. Pre-deoxygenated 1,4-dioxane (15 mL) solution and K₂CO₃ (2 M 2.0 mL) solution were injected into the flask. The reaction was reflux at 90 °C for 12 h. After monitoring the reaction, the system was cooled to room temperature, extracted with dichloromethane (DCM), and dried with anhydrous Na₂SO₄ for 3 h. After vacuum extraction and filtration, the most of the

solvent was removed using a rotary evaporator. Finally, the crude product was purified by column chromatography on silica gel (eluent: EA:PE = 1:5) to obtain white solid powder (249.6 mg, yield: 83.18%). ¹H NMR (600 MHz, DMSO) δ 7.75, 7.73, 7.73, 7.73, 7.72, 7.67, 7.66, 7.58, 7.57, 7.56, 7.55, 7.36, 7.34, 7.12, 7.11, 7.10, 7.10, 6.89, 6.87, 6.83, 6.81, 3.69, 3.33, 2.50. ¹³C NMR (151 MHz, DMSO) δ 154.81, 145.84, 142.37, 141.91, 137.39, 137.09, 135.46, 134.23, 132.15, 131.14, 130.20, 128.59, 126.86, 124.96, 124.45, 124.02, 122.10, 121.39, 119.69, 116.94, 115.15, 111.18, 55.63.

2. Figures

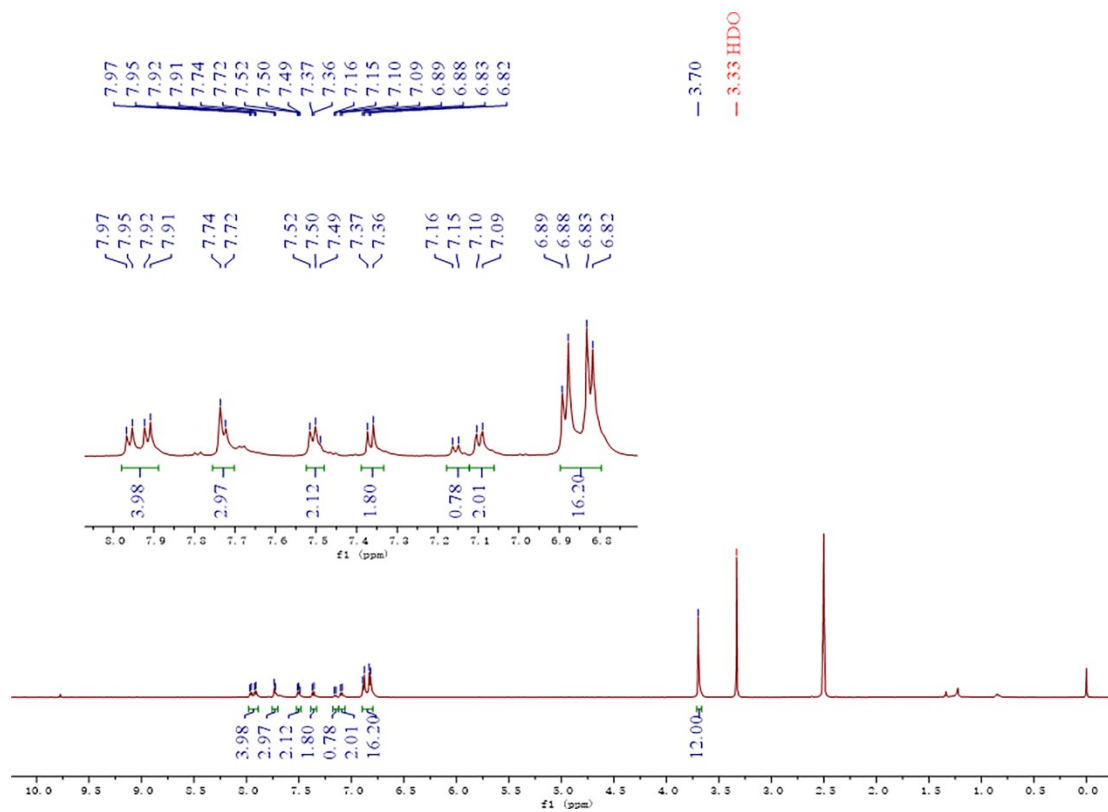


Figure. S2 ^1H NMR spectrum of JY4 in DMSO.

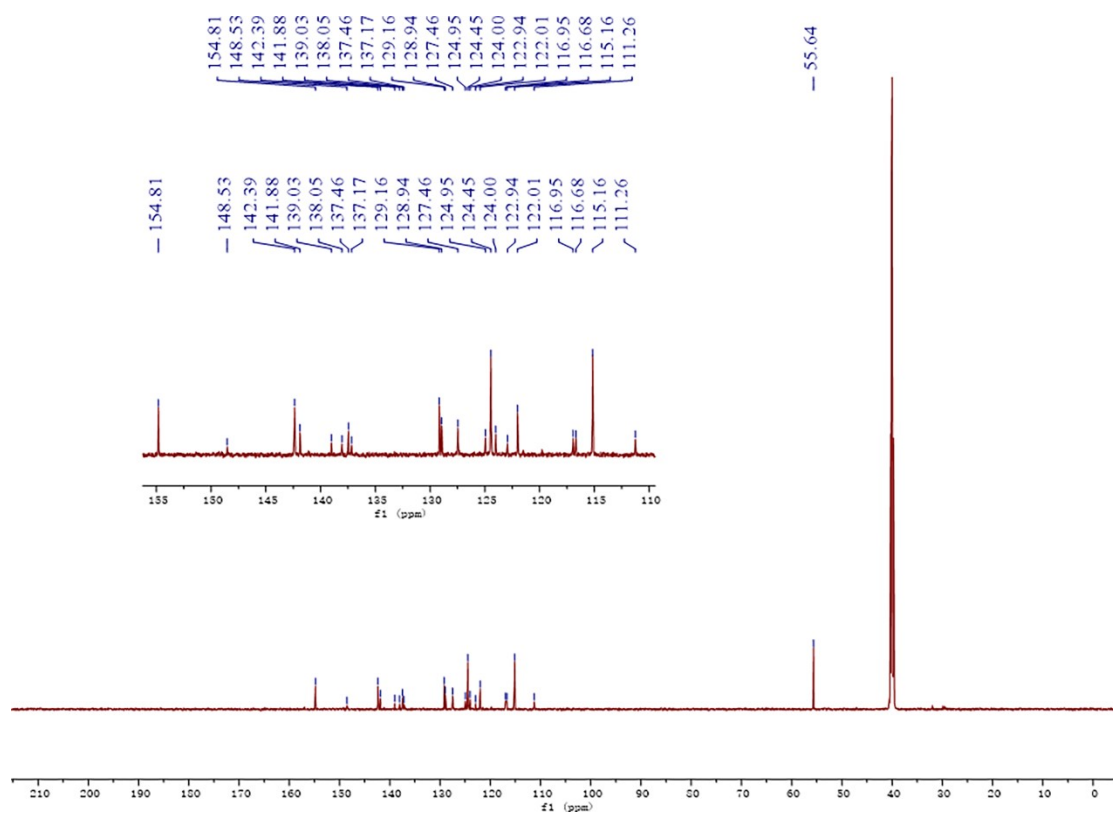


Figure. S3 ^{13}C NMR spectrum of JY4 in DMSO.

Mass Spectrum Deconvolution Report

Analysis Info

Acquisition D 2023/7/27 09:00:00
14:44:43

Analysis Name C:\Users\Administrator\Desktop\HRMS\JY4.d

Method DirectInfusion - MS - positive.m

Operator Demo User

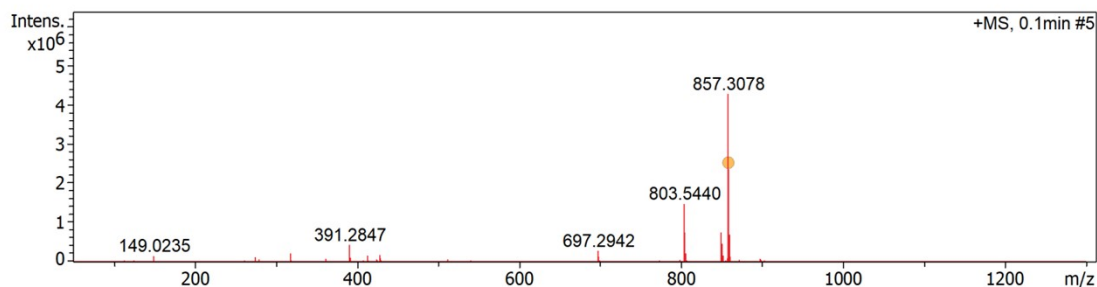
Sample Name Fmoc-Ile-Thr (tBu)-OH

Instrument impact II 1825265.1022
1

Comment

Acquisition Paramet

Source Type	ESI	Ion Polarity	Positive	Set Nebulizer	0.4 Bar
Focus	Active	Set Capillary	4500 V	Set Dry Heater	180 °C
Scan Begin	50 m/z	Set End Plate	-500 V	Set Dry Gas	4.0 l/min
Scan End	1300 m/z	Set Charging	2000 V	Set Divert Valve	Source
		Set Corona	0 nA	Set APCI Heater	0 °C



Component	Molecular Mass	Molecule	Absolute Abundance	Relative Abundance
-----------	----------------	----------	--------------------	--------------------

MASS SPECTROMETRY REPORT

Sample No.	Formula (M)	Measured m/z	Calc. m/z	Diff (ppm)
JY4	C53H42F3N3O5	857.3078	857.3077	0.12

Figure. S4 High resolution mass spectrometry of JY4.

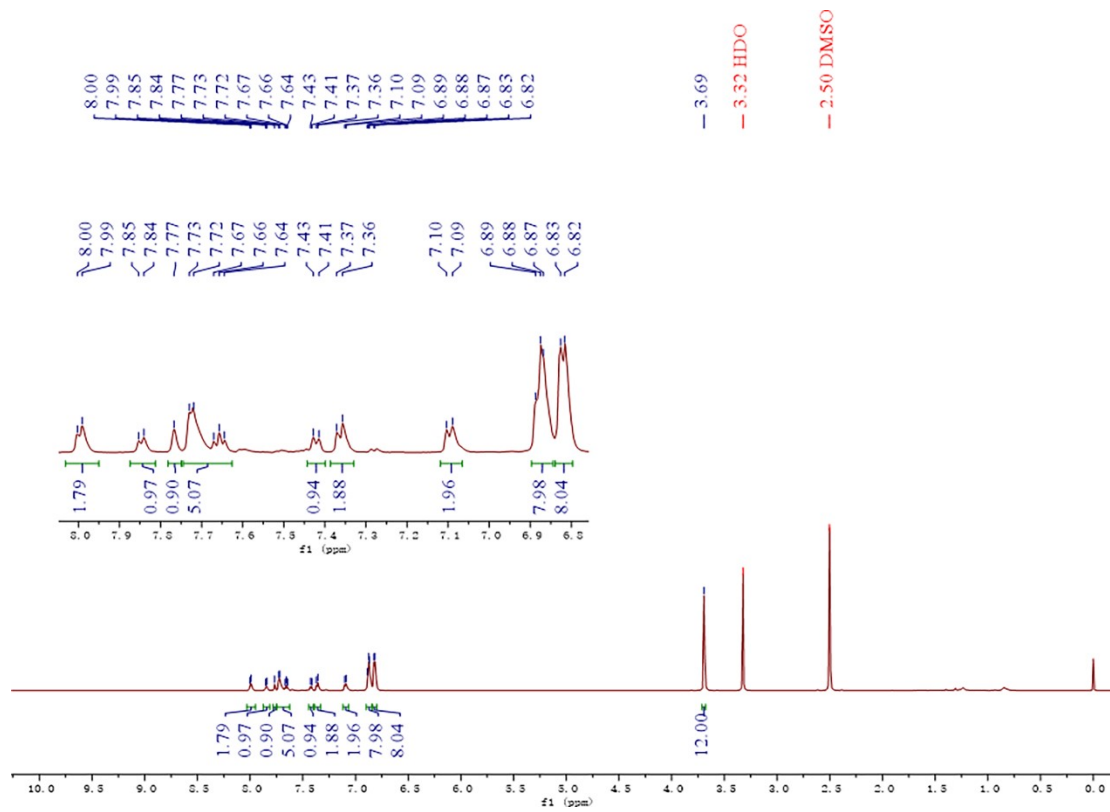


Figure. S5 ^1H NMR spectrum of JY5 in DMSO.

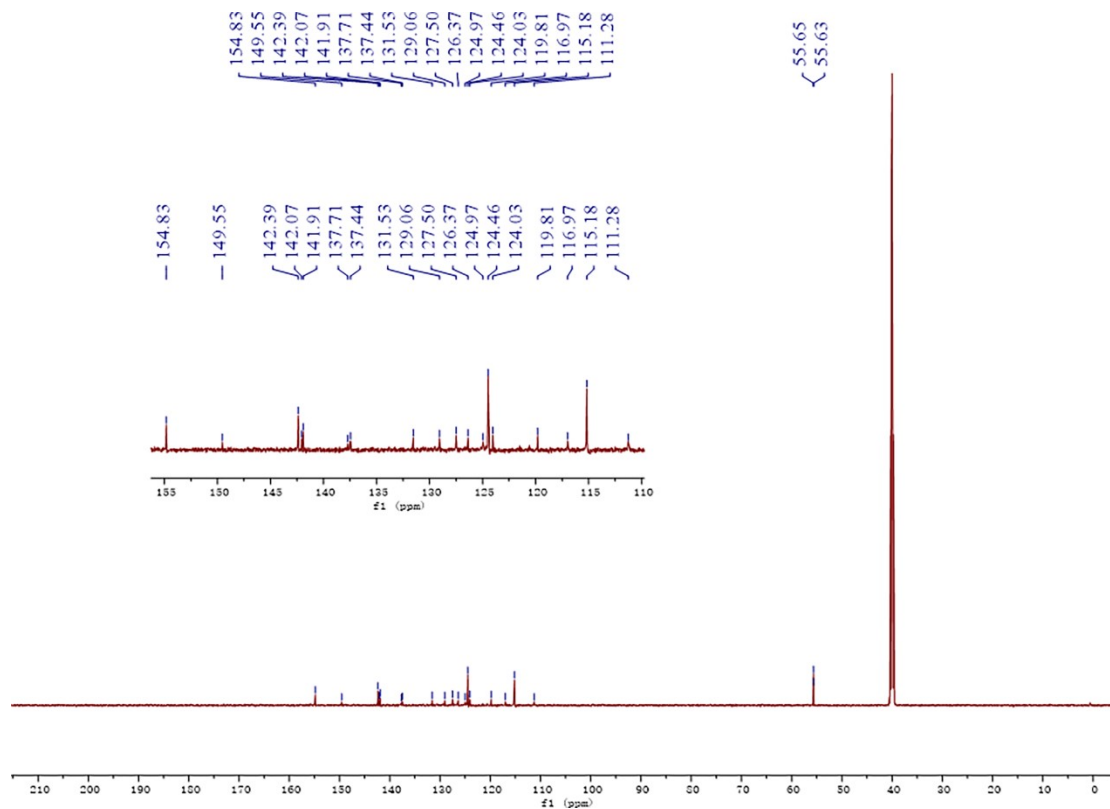


Figure. S6 ^{13}C NMR spectrum of JY5 in DMSO.

Mass Spectrum Deconvolution Report

Analysis Info

Acquisition D 2023/7/27 08:00:00
14:45:39

Analysis Name C:\Users\Administrator\Desktop\HRMS\JY5.d

Method DirectInfusion - MS - positive.m

Operator Demo User

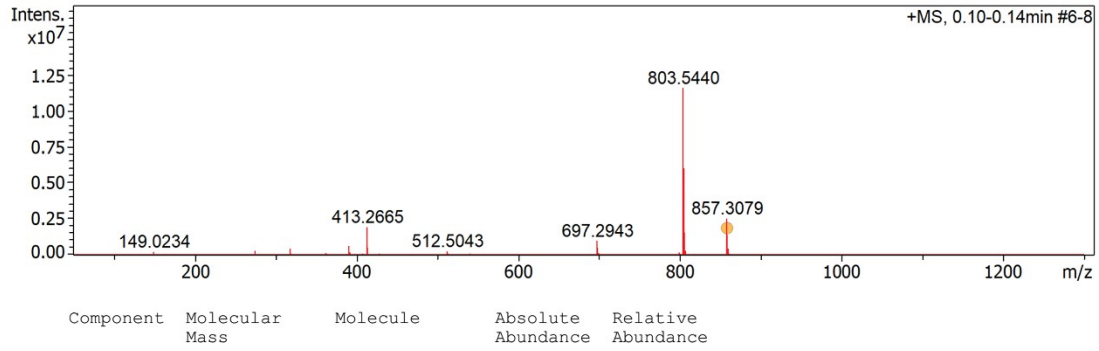
Sample Name Fmoc-Ile-Thr (tBu)-OH

Instrument impact II 1825265.1022
1

Comment

Acquisition Paramet

Source Type	ESI	Ion Polarity	Positive	Set Nebulizer	0.4 Bar
Focus	Active	Set Capillary	4500 V	Set Dry Heater	180 °C
Scan Begin	50 m/z	Set End Plate	-500 V	Set Dry Gas	4.0 l/min
Scan End	1300 m/z	Set Charging	2000 V	Set Divert Valve	Source
		Set Corona	0 nA	Set APCI Heater	0 °C



MASS SPECTROMETRY REPORT

Sample No.	Formula (M)	Measured m/z	Calc. m/z	Diff (ppm)
JY5	C53H42F3N3O5	857.3079	857.3077	0.23

Figure. S7 High resolution mass spectrometry of JY5.

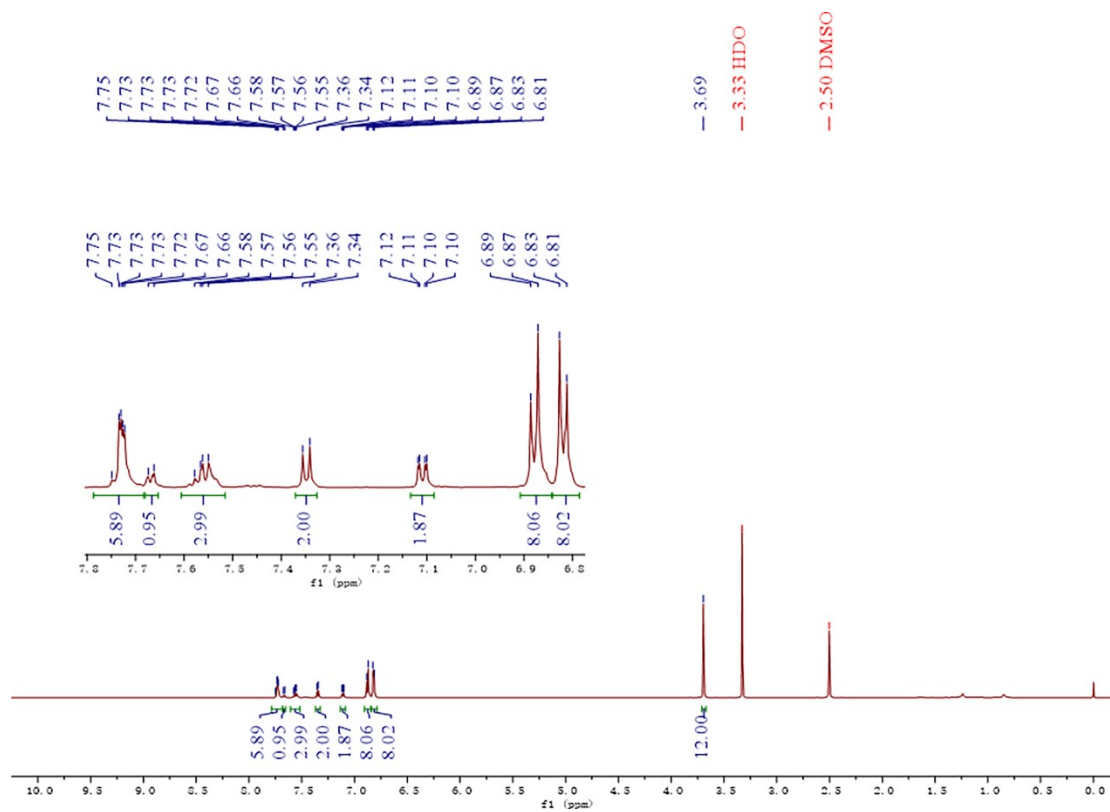


Figure. S8 ^1H NMR spectrum of JY6 in DMSO.

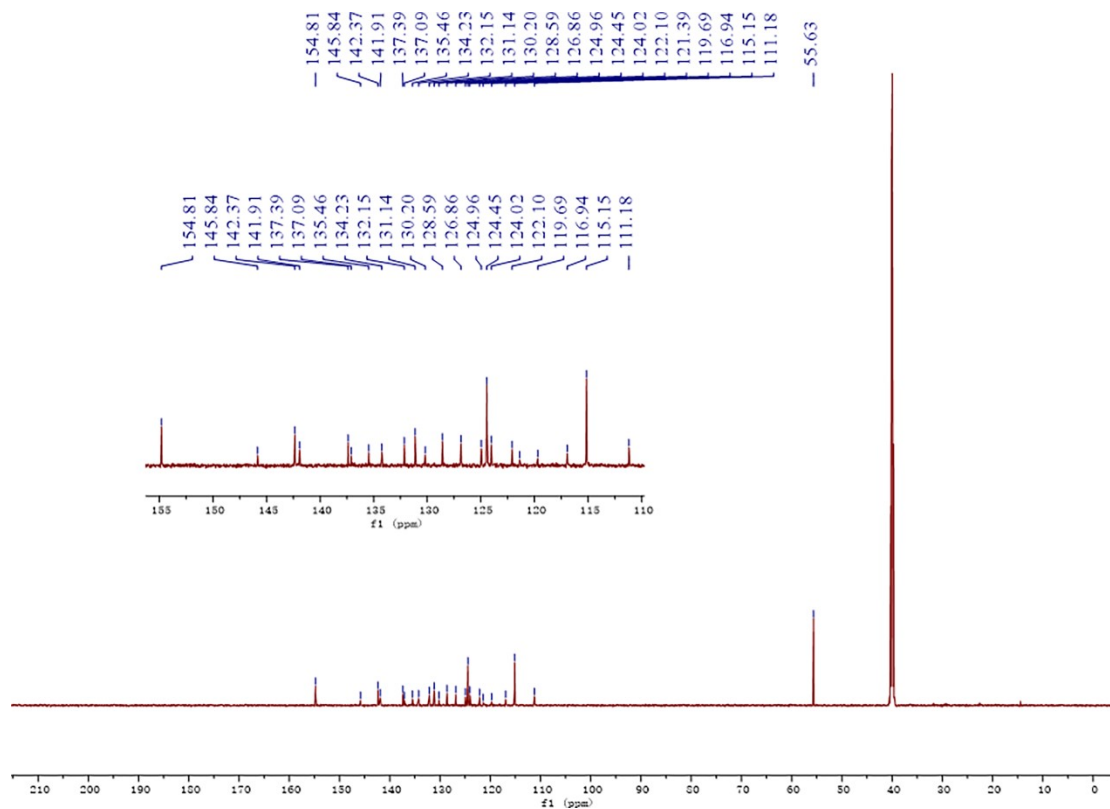


Figure. S9 ^{13}C NMR spectrum of JY6 in DMSO.

Mass Spectrum Deconvolution Report

Analysis Info

Acquisition D 2023/7/27 09:00:00
14:46:39

Analysis Name C:\Users\Administrator\Desktop\HRMS\JY6.d

Method DirectInfusion - MS - positive.m

Operator Demo User

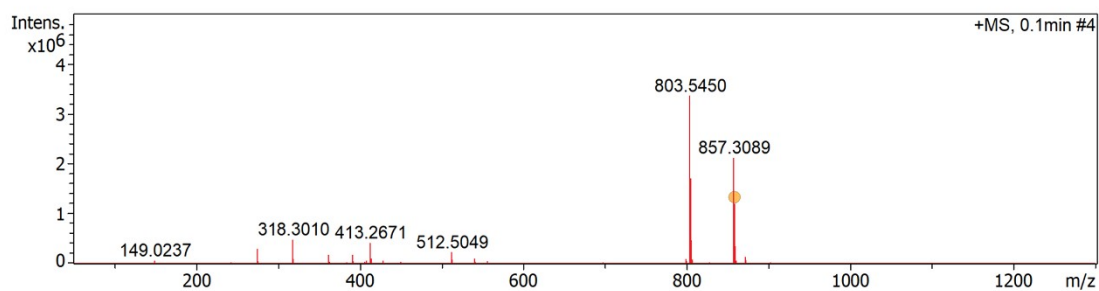
Sample Name Fmoc-Ile-Thr (tBu)-OH

Instrument impact II 1825265.1022
1

Comment

Acquisition Paramet

Source Type	ESI	Ion Polarity	Positive	Set Nebulizer	0.4 Bar
Focus	Active	Set Capillary	4500 V	Set Dry Heater	180 °C
Scan Begin	50 m/z	Set End Plate	-500 V	Set Dry Gas	4.0 l/min
Scan End	1300 m/z	Offset	2000 V	Set Divert Valve	Source
		Wet Gas	0 nA	Set APCI Heater	0 °C



Component	Molecular Mass	Molecule	Absolute Abundance	Relative Abundance
-----------	----------------	----------	--------------------	--------------------

MASS SPECTROMETRY REPORT

Sample No.	Formula (M)	Measured m/z	Calc. m/z	Diff (ppm)
JY6	C₅₃H₄₂F₃N₃O₅	857.3089	857.3077	1.40

Figure. S10 High resolution mass spectrometry of JY6.

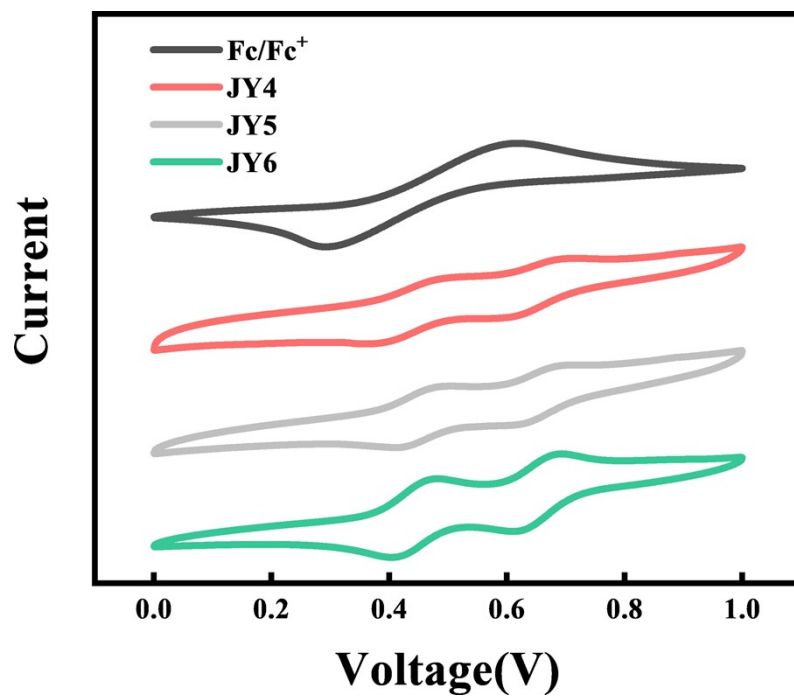


Figure. S11 Cyclic voltammetry curve of JY4, JY5, and JY6.

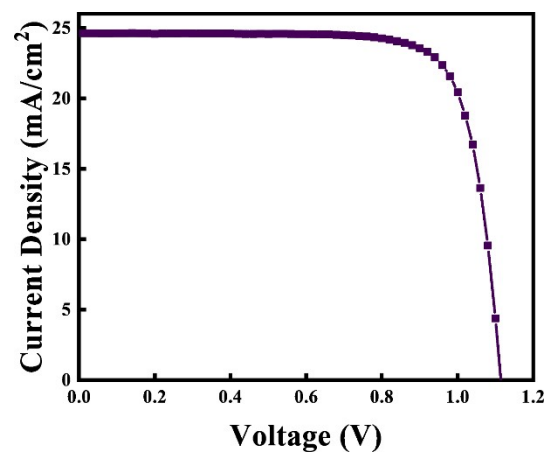


Figure. S12 J - V curves of Spiro-OMeTAD based device.

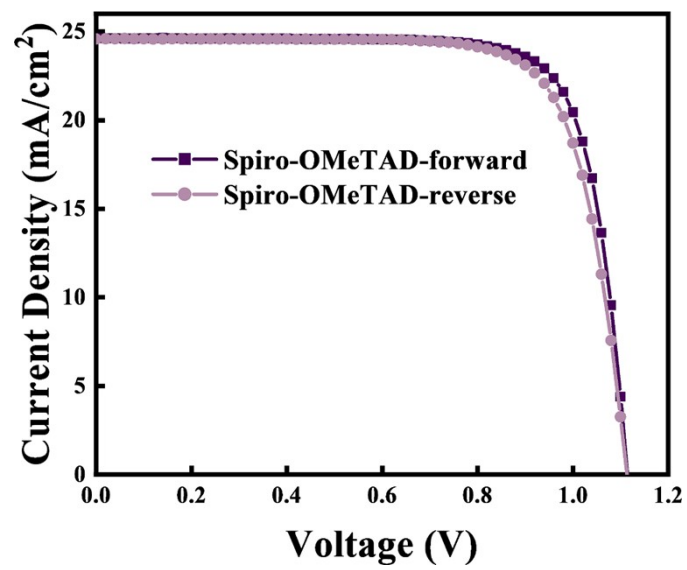


Figure. S13 $J-V$ curves under reverse and forward scan for Spiro-OMeTAD based PSCs device.

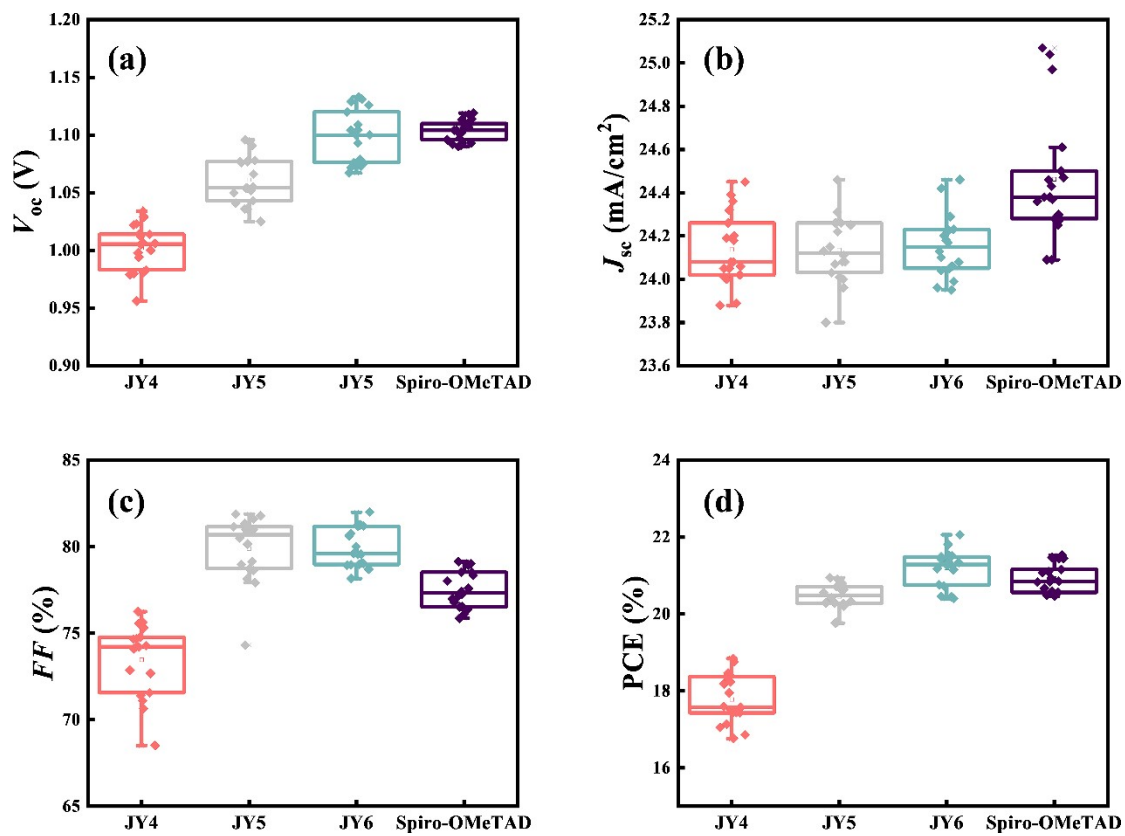


Figure. S14 Box charts of the photovoltaic parameters of HTMs.

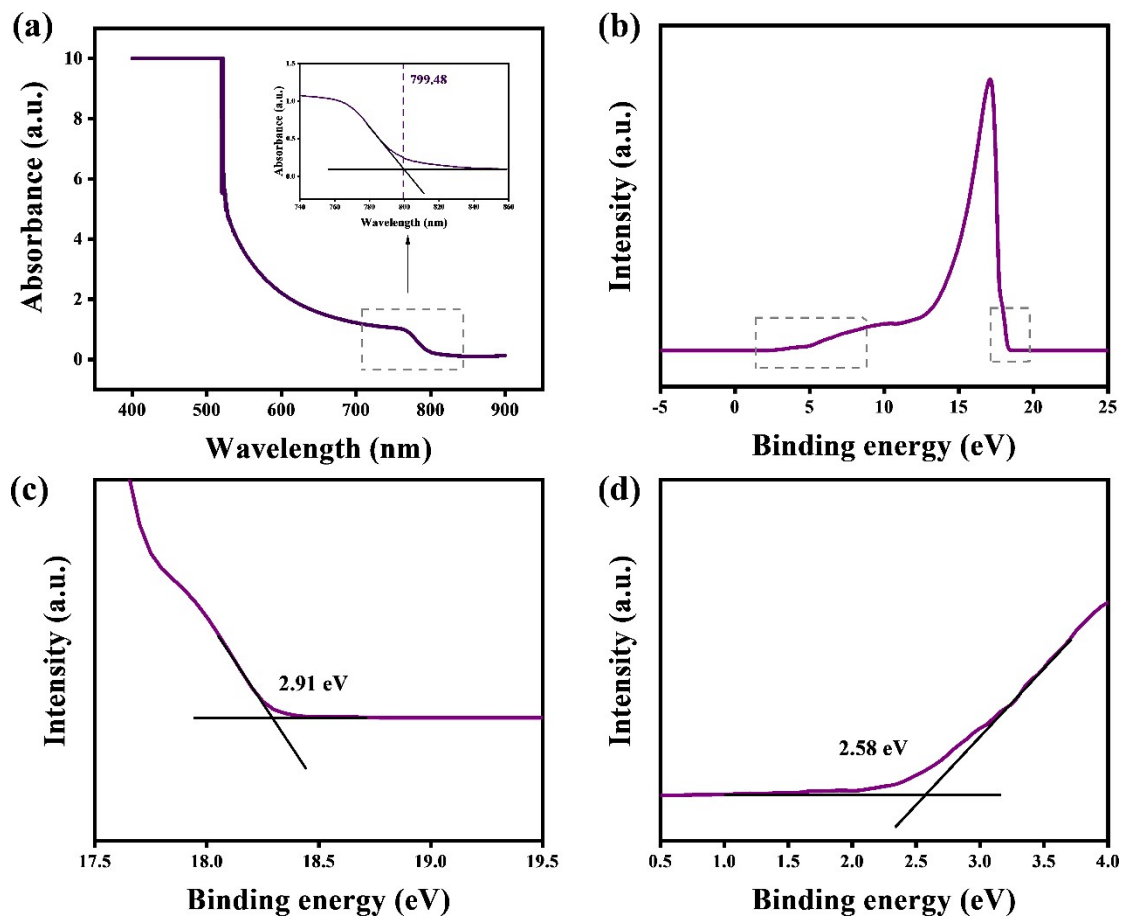


Figure. S15 (a) UV-vis absorption spectra of perovskite films (b) UPS spectra of perovskite film. (c) The secondary electron cut-off region. (d) Magnified spectra near Fermi edge.

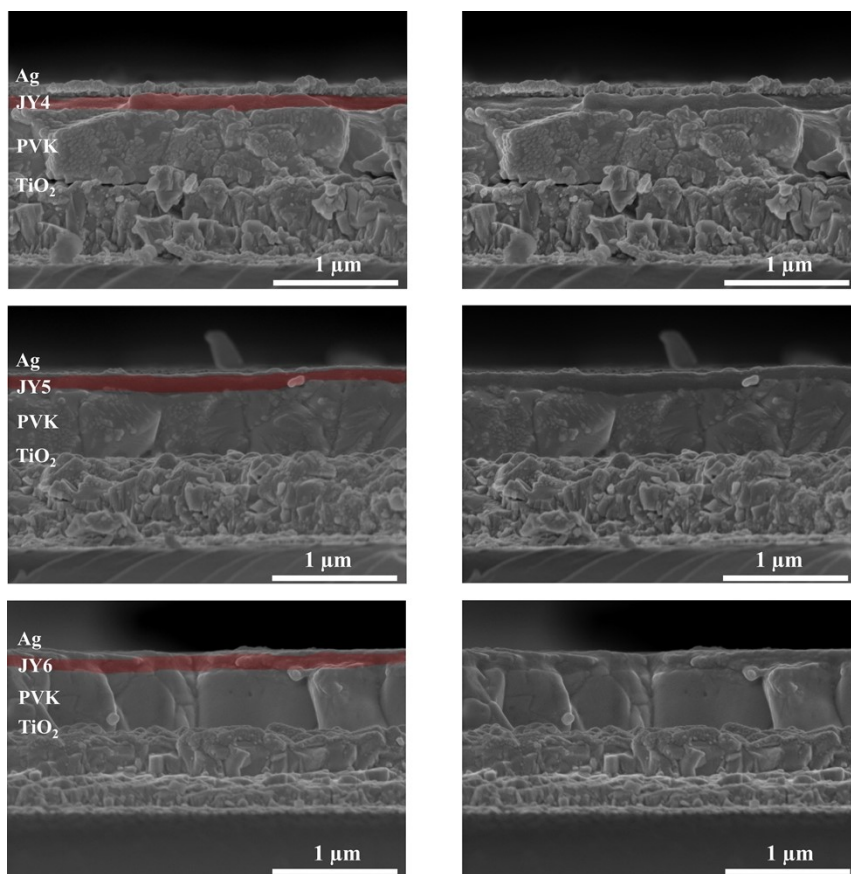


Figure. S16 Cross-sectional SEM images of the PSC devices with HTM concentrations of 50mg/mL for JY4-JY6.

2.3 Tables

Table S1. Interaction energy between HTMs and perovskite.

	Coul-SR [kJ/mol]	LJ-SR [kJ/mol]	E_{in} [kJ/mol]
JY4/PVK	-162.50	-709.21	-871.71
JY5/PVK	-157.08	-808.97	-966.05
JY6/PVK	-187.66 ^{a)}	-886.61 ^{b)}	-1074.27 ^{c)}

^{a)} The electrostatic interaction between the HTM and the perovskite; ^{b)} The van der Waals interaction between the HTM and the perovskite; ^{c)} Interaction between HTM and perovskite.

Table S2. Interface adsorption energy of three molecules.

	E_{PVK}	$E_{\text{PVK/HTM}}$	E_{HTM}	E_{ads} [eV]
JY4	-2984.17	-3686.73	-699.49	-3.07
JY5	-2984.12	3686.32	-699.09	-3.12
JY6	-2984.20	-3686.19	-698.72	-3.27

Table S3 Photovoltaic parameters of Spiro-OMeTAD based PSCs devices.

HTMs	V_{OC} [V]	J_{SC} [mA/cm ²]	FF [%]	PCE [%]
Spiro-OMeTAD	1.114 (1.103±0.009)	24.61 (24.46±0.29)	78.53 (77.5±1.05)	21.53 ^{a)} (20.92±0.37) ^{b)}

^{a)} The maximum value; ^{b)} The average value was obtained from 18 devices.

Table S4. Summary of hysteresis index (HI) and device performance of perovskite solar cell adopting JY4, JY5 and JY6 at forward and reverse voltage scans.

HTM		V_{oc} [V]	J_{sc} [mA/cm ²]	FF [%]	PCE [%]	HI ^{a)} [%]
JY4	forward	1.034	24.08	75.64	18.84	5.10
	reverse	1.030	24.08	72.09	17.88	
JY5	forward	1.077	24.15	80.51	20.94	3.82
	reverse	1.071	24.14	77.90	20.14	
JY6	forward	1.100	24.46	81.99	22.06	3.17
	reverse	1.100	24.40	79.58	21.36	
Spiro-OMeTAD	forward	1.114	24.61	78.53	21.53	3.16
	reverse	1.113	24.58	75.84	20.85	

^{a)} $HI = [(PCE_{forward} - PCE_{reverse}) / PCE_{forward}] \times 100\%$

Table S5. JY4 based PSCs device concentration optimization of photovoltaic parameters.

JY4 (mg/mL)	V_{oc} (V)	J_{sc} (mA/cm ²)	FF (%)	PCE (%)
40	1.004	24.29	71.43	17.42
50	1.034	24.08	75.64	18.84
60	1.022	24.04	74.24	18.24

Table S6. JY5 based PSCs device concentration optimization of photovoltaic parameters.

JY5 (mg/mL)	V_{oc} (V)	J_{sc} (mA/cm ²)	FF (%)	PCE (%)
40	1.075	24.26	74.12	19.33
50	1.077	24.15	80.51	20.94
60	1.079	24.18	77.88	20.32

Table S7. JY6 based PSCs device concentration optimization of photovoltaic parameters.

JY6 (mg/mL)	V_{oc} (V)	J_{sc} (mA/cm ²)	FF (%)	PCE (%)
40	1.072	24.40	77.88	20.37
50	1.100	24.46	81.99	22.06
60	1.120	24.07	78.94	21.28

Table S8 The film thickness of JY4-JY6 at different concentrations.

	JY4 (nm)	JY5 (nm)	JY6 (nm)
40 mg/mL	68.9	78.9	79.1
50 mg/mL	100.7	112.42	116.48
60 mg/mL	145.5	157.7	159.8

References

- 1 S. Ghosh, P. Verma, C. J. Cramer, L. Gagliardi and D. G. Truhlar, *Chem. Rev.*, 2018, **118**, 7249–7292.
- 2 X. Liu and X. Liu, *RSC Adv.*, 2019, **9**, 24733–24741.
- 3 M. J. Frisch, G. W. Trucks, H. B. Schlegel, G. E. Scuseria, M. A. Robb, J. R. Cheeseman, G. Scalmani, V. Barone, G. A. Petersson, H. Nakatsuji, X. Li, M. Caricato, A. Marenich, J. Bloino, B. G. Janesko, R. Gomperts, B. Mennucci, H. P. Hratchian, J. V. Ortiz, A. F. Izmaylov, J. L. Sonnenberg, D. Williams-Young, F. Ding, F. Lipparini, F. Egidi, J. Goings, B. Peng, A. Petrone, T. Henderson, D. Ranasinghe, V. G. Zakrzewski, J. Gao, N. Rega, G. Zheng, W. Liang, M. Hada, M. Ehara, K. Toyota, R. Fukuda, J. Hasegawa, M. Ishida, T. Nakajima, Y. Honda, O. Kitao, H. Nakai, T. Vreven, K. Throssell, J. A. Montgomery, Jr., J. E. Peralta, F. Ogliaro, M. Bearpark, J. J. Heyd, E. Brothers, K. N. Kudin, V. N. Staroverov, T. Keith, R. Kobayashi, J. Normand, K. Raghavachari, A. Rendell, J. C. Burant, S. S. Iyengar, J. Tomasi, M. Cossi, J. M. Millam, M. Klene, C. Adamo, R. Cammi, J. W. Ochterski, R. L. Martin, K. Morokuma, O. Farkas, J. B. Foresman, and D. J. Fox, Gaussian 09, revision A.01. Wallingford, CT: Gaussian, Inc.; 2009.
- 4 D. Van Der Spoel, E. Lindahl, B. Hess, G. Groenhof, A. E. Mark and H. J. C. Berendsen, *J. Comput. Chem.*, 2005, **26**, 1701–1718.
- 5 C. I. Bayly, P. Cieplak, W. Cornell and P. A. Kollman, *J. Phys. Chem.*, 1993, **97**, 10269–10280.
- 6 J. Wang, R. M. Wolf, J. W. Caldwell, P. A. Kollman and D. A. Case, *J. Comput. Chem.*, 2004, **25**, 1157–1174.
- 7 W. Humphrey, A. Dalke and K. Schulten, *Journal of Mol. Graph.*, 1996, **14**, 33–38.
- 8 T. Lu and F. Chen, *J. Comput. Chem.*, 2012, **33**, 580–592.
- 9 R. A. Marcus, *Annu. Rev. Phys. Chem.*, 1964, **15**, 155–196.
- 10 V. Coropceanu, J. Cornil, D. A. Da Silva Filho, Y. Olivier, R. Silbey and J.-L. Brédas, *Chem. Rev.*, 2007, **107**, 926–952.
- 11 K. Senthilkumar, F. C. Grozema, F. M. Bickelhaupt and L. D. A. Siebbeles, *J. Chem. Phys.*, 2003, **119**, 9809–9817.
- 12 W.-Q. Deng and W. A. Goddard, *J. Phys. Chem. B*, 2004, **108**, 8614–8621.
- 13 G. Te Velde, F. M. Bickelhaupt, E. J. Baerends, C. Fonseca Guerra, S. J. A. Van Gisbergen, J. G. Snijders and T. Ziegler, *J. Comput. Chem.*, 2001, **22**, 931–967.
- 14 C. Fonseca Guerra, J. G. Snijders, G. Te Velde and E. J. Baerends, *Theor. Chem. Acc.*, 1998, **99**, 391–403.
- 15 G. Kresse and J. Furthmüller, *Comput. Mater. Sci.*, 1996, **6**, 15–50.
- 16 G. Kresse and J. Furthmüller, *Phys. Rev. B*, 1996, **54**, 11169–11186.
- 17 J. P. Perdew, K. Burke and M. Ernzerhof, *Phys. Rev. Lett.*, 1996, **77**, 3865–3868.
- 18 J. P. Perdew, J. A. Chevary, S. H. Vosko, K. A. Jackson, M. R. Pederson, D. J. Singh and C. Fiolhais, *Phys. Rev. B*, 1992, **46**, 6671–6687.